EXPERIMENTAL AND NUMERICAL COMPARISON OF HEAT TRANSFER IN A NATURALLY VENTILATED ROOF CAVITY

Adrien Brun[1], Etienne Wurtz[1], and Daniel Quenard[2]
[1]LOCIE,CNRS FRE 3220, INES-RDI, Université de Savoie, Le Bourget du Lac, France
[2]Centre Scientifique et Technique du Bâtiment (CSTB), 38400 St-Martin dHères, France

ABSTRACT

Timber-frame structures can be built with a closed cavity or an open naturally ventilated cavity (Open Cavity, OC). An open cavity reduces the risk of moisture damaging the structure. OCs are generally not considered in thermal behavior simulation software, although there is much research that shows it can improve thermal comfort. The aim of this work is to develop a numerical model for a naturally ventilated cavity that is also sufficiently accurate for year-long thermal simulation in buildings. To this end, we built a full-scale experimental setup consisting of two identical rooms (the same dimensions, orientation, material etc.) in order to compare, under real climatic conditions, an unventilated cavity (Closed Cavity) with a naturally ventilated one (OC). The experimental setup was installed at the scientific and technical building research center (CSTB) in Grenoble (France). The experimental results were used to validate and improve a simple mathematical model. The numerical simulations were carried out with SPARK (Lawrence-Berkeley-National-Laboratory and Ayres-Sowell-Associates 2003).

INTRODUCTION

In the literature, a number of works demonstrate the improvement of thermal comfort by the use of a gap between elements in the walls of the building. Two main techniques are used : solar-assisted natural ventilation (FIGURE 1a) and the reduction of solar energy transmission through the building envelope (FIGURE 1b).

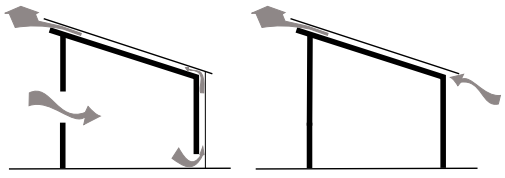

(a) Enhancing ventilation (b) Heat-transfer limitation

FIGURE *1: Inter-space and summer comfort improvement.*

Current guidelines for roofs and timber-frame require external and internal layers to be separated by a ventilated layer to prevent damage to the structure. Our work focuses on the thermal interest of this type of construction.

Building ventilation rates can be increased by using a solar chimney. The chimney is generally integrated in the building envelope and consists of a transparent material (usually glazing), an air cavity and an absorber. The absorber heats the air by convection. The air density difference between heated and external air induces natural ventilation. (For an example of integration in a roof, see "Roof Solar Collector, RSC" (Khedari et al. 2000), (Hirunlabh et al. 2001), of wall integration "Metallic Solar Walls MSW" (Hirunlabh et al. 1999) and made up vertical and inclined parts (AboulNaga and Abdrabboh 2000)). Since the internal wall generally does not have a high thermal storage capacity, (MartIHerrero and HerasCelemin 2007) studied the association of a solar chimney with a concrete wall in order to provide natural ventilation at night for a Mediterranean climate. (Aboulnaga 1998) assessed a solar chimney coupled with adiabatic cooling which naturally ventilates and cools a building. Airflow rates can also be enhanced by adding, at the chimney outlet, a wind-driven system that maintains lower pressure for all wind directions (Bansal, Mathur, and Bhandari 1994), (Khan, Su, and Riffat 2008).

A gap between the elements of the building envelope can also be used to limit heat flux though the walls. The covering is generally made of a non-transparent layer (metal, wood, canvas). Natural convection induced by heat convective exchange between covering and internal air can eliminate part of the absorbed solar heat. The upper and lower sides are often covered with a Radiant Barrier System (RBS) (low emissivity layers) which limit the radiative heat transfer (Chami 2009), (Miranville 2002).

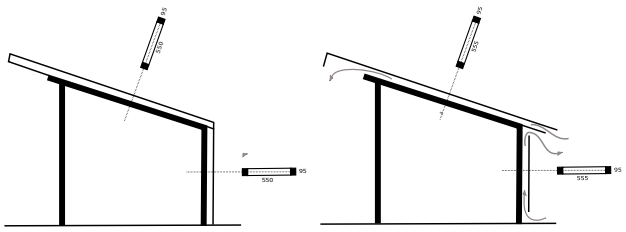

(a) Closed Cavity (CC) (b) Opened Cavity (OC)

FIGURE *2: The studied configurations*

Current guidelines for roofs and timber-frame structures ((DTU-41.2 1996), (DTU-31.2 1993)) recommend separating the external and internal layers by means of a

ventilated gap particularly to avoid damage to the structure, while the present work focuses on the thermal consequences of this type of system.

For this purpose, thermal evaluation of the naturally ventilated cavity was assessed using a full-scale experimental setup consisting of two identical rooms which include in their south facade either an open (FIGURE 2b) or a closed cavity (FIGURE 2a).

The experimental comparison is based on a 48-hour recording sample. A simple mathematical model, already used in previous works ((Bansal, Mathur, and Bhandari 1994),(Brinkworth, Marshall, and Ibarahim 2000)) is presented. Finally, the numerical and experimental results are compared.

EXPERIMENTAL SET-UP

FIGURE *3: Experimental setup under construction*

Prototype

The experimental study was conducted at the CSTB (The French Scientific and Technical Research Center). The CSTB is located at 45°11'7.52" North and 5°46'24.97" East, in Grenoble (France).

The experimental set-up is shown in FIGURES 4, 3 & 5. It is a south-facing house with two identical rooms and an inclined roof (angle of inclination : 30°). Both rooms have the same dimensions, materials, components, and instrumentation. In this paper, the study concentrated on a part of the roof and the front wall as shown in FIGURES 4 (region marked red).

The setup has a simple rectangular duct section measuring 550 mm x 95 mm. The upper plate consists of a black sealing coat and 10 mm Oriented Strand Boad (OSB). The bottom plate consists of a Radiant Barrier Layer (RBL) which significantly reduces thermal radiation, 10 mm OSB, 90 mm of insulation and a vapor barrier.

During the experiment, two solutions were proposed ; one with an Open Cavity (OC) on the east room, the other with a Closed Cavity (CC) on the west room. The other

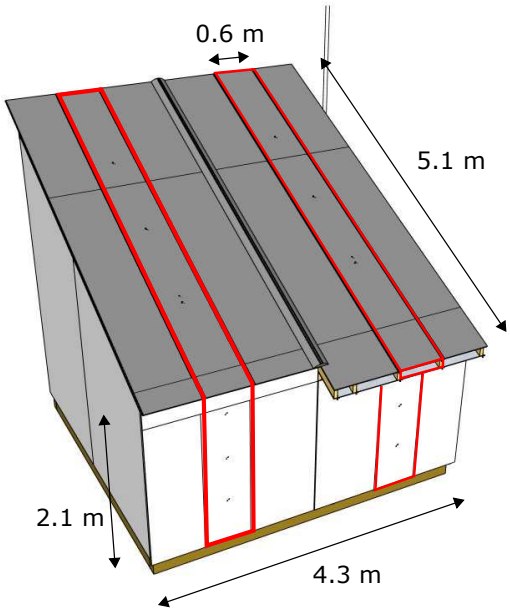

FIGURE *4: South- facing wall and roof*

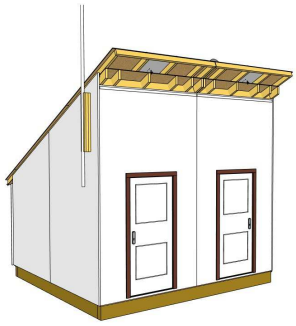

FIGURE *5: North wall of the experimental set up*

surfaces (vertical walls, floor and partitions) were well insulated (200 mm layer of fiber glass) and covered with white gypsum plaster.

Instrumentation

T-Type thermocouples were used to measure the temperature along the central axis of the inner surfaces in the cavity. For OC (respectively CC) these measurements were taken on the upper and lower surfaces (B & D), at the centre of cavity (C) at 50,170,290,410 and 510 cm (above the floor) from the inlet (respectively 0,120,240,360 and 460 cm). Flux meters (50mm × 50mm, Captec) were used to measure convective and radiative components on both sides of the cavity. This type of flux sensor also contains an integrated thermocouple which also allows temperature measurement. On the upper plate, the same surface emissivity is obtained by painting the sensor, while, on the

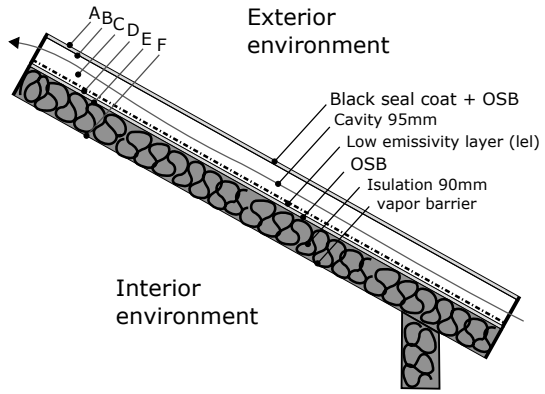

FIGURE *6: Schematic diagram of the South wall-type. Layer indication and building materials description*

lower plate, it is placed between the RBL and the OSB.

For vertical and inclined cavities, the inlet/outlet pressure difference was measured by using two Furness FCO332 pressure transmitters. FIGURE 17 shows the positions of the sensors.

Vaisala WXT-510 recorded the most essential weather parameters at 6 m above the ground (wind velocity and direction, liquid precipitation, barometric pressure, temperature and relative humidity). A photodiode detector was used to measure overall horizontal solar radiation.

Each internal surface temperature and the air temperature at 2 different heights above the ground were recorded.

All the experimental data were logged through a Campbell CR1000 data logger connected to the CSTB local network. By using the CR1000, coupled to a number of multiplexers (AM16/32 and AM25T), it was possible to provide 162 differential measurement channels. All the data were recorded every minute ; the 5-minute data averages are presented here.

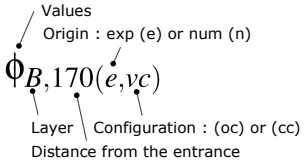

FIGURE *7: Notation nomenclature*

EXPERIMENTAL RESULTS

The first available experimental sequence is presented here. It concerns 2 days in September 2009 in fairly hot weather conditions. FIGURE 8 shows these conditions, including direct solar radiation, external temperature and pressure difference ΔP_{tilted}.

FIGURE 9 shows the air and the upper surface temperature at 290 cm from the entrance. Dotted lines indicate data collected every minute and continuous lines, the 5

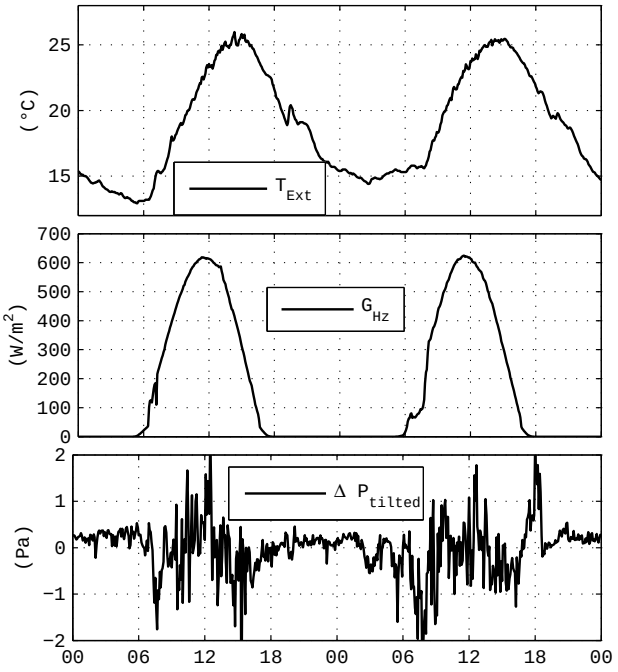

FIGURE *8: Measured external temperature, solar radiation and pressure difference for two days of clear weather*

minute averages. These plots highlight the fluctuating nature of the internal temperature over a range of +/- 2.5 $^{\circ}C$ around the average. Due to their thermal inertia, surface temperatures are less sensitive to these fluctuations (range of +/- 1 $^{\circ}C$).

A typical set of data for the upper and bottom plates and the air gap is shown in FIGURE 10 and FIGURE 11. It can be seen that the upper plate temperature is about twenty degrees higher than the bottom plate in the case of the open cavity.

We noted limited temperature differences between the core air gap and the lower face. Observations were also recorded by (Ong and Chow 2003), (Sakonidou et al. 2008), investigations in which temperature measurements at various distances from the heated plate were made. (In these temperature profiles across a 100 mm air gap, it is seen that the greatest gradient is in the first 20 mm air layer from the absorber plate.)

Generally, the temperature increased with increased distance from the cavity inlet. It was observed that near the outlet, the temperature tends to decrease. This drop in air and surfaces temperature could be attributed to the mixing of external and internal air and the changes of boundary conditions in the lower side. A comparison of the configurations shows that temperatures of the non-ventilated cavity are on the inner side about fifteen degrees higher than the ventilated cavity.

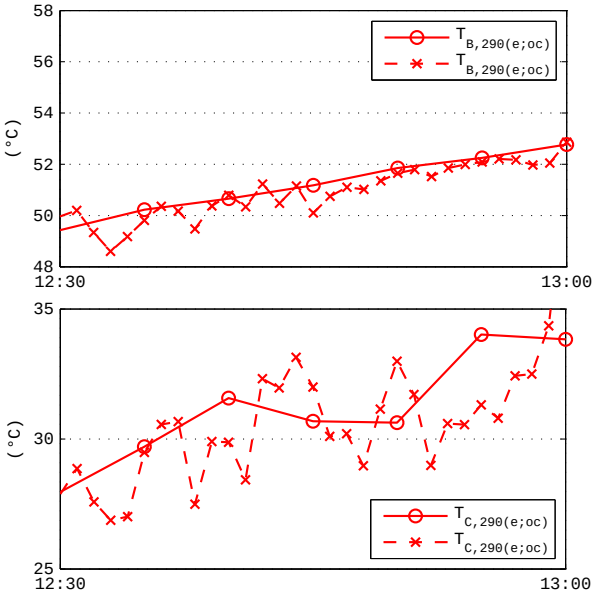

FIGURE *9: 28/09/2009, OC configuration : Temperature variation in layers B (upper graph) and C (lower graph) recorded at one-minute intervals (continuous lines) and 5-minute averages (dotted lines)*

FIGURE 12 compares the measured heat flux on both sides of the cavity for ventilated and non-ventilated cavities. It was found that the natural ventilation in the cavity reduced the heat gain through the ceiling by about 40-50 %. The much greater heat transfer on the upper side is explained by the fact that more absorbed heat was transferred to the air channel.

Finally, while the temperature on the ceiling surfaces (T_F) was considered in these two configurations (FIGURE 13) we noted that in the case of the ventilated cavity, its amplitude could be reduced by 1 $^{\circ}C$. It should be remembered that there is no release of internal heat, no solar contribution and no internal ventilation in the volume.

MATHEMATICAL MODELING

Following the work of (Hirunlabh et al. 1999), (Bansal, Mathur, and Bhandari 1994), a similar mathematical model was developed for estimating heat gain throughout the inner part of the naturally ventilated component. The following assumptions were made regarding the equations :

- One-dimensional heat transfer : temperature, heat flux, thermo-physical properties etc. as well as the width and length of the channel were assumed to be constant.
- Air acts as a non-radiation absorbing fluid.
- Adimensional numbers are evaluated at film temperature.

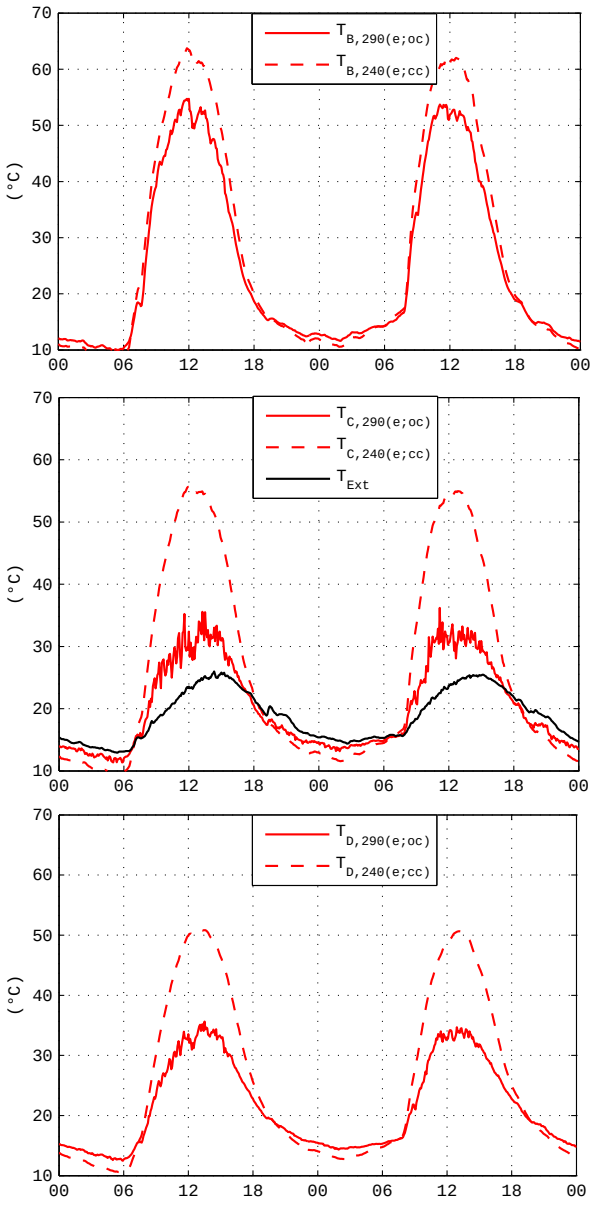

FIGURE *10: Air temperature variation recorded in 3 layers (B : upper surface temperature, C : core air temperature and D : lower air temperature) at 290 cm from the inlet for the open configuration (red) and at 240cm for the closed cavity (doted red)*

- Air density is dependant only on temperature (Boussinesq approximation : $(\rho_{ref} - \rho(z) = \rho_M \beta (T_f(z) - T_{ref}))$.
- The side surface of the cavity is not considered in the heat-transfer mechanism.
- External air temperature differences between inlet and outlet are negligible.
- The unity view factor is assumed between parts of

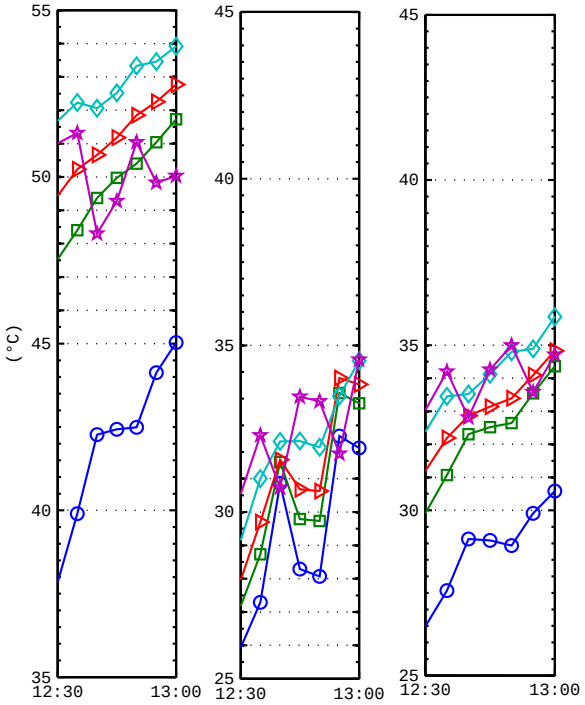

FIGURE *11: 28/09/2009, OC configuration : From left to right, temperature measurements on layers B, C and D at various distances from the inlet (blue-circle : 50cm, green-square : 170, red-triangle : 290, light blue-diamond : 410 and purple-star : 510cm)*

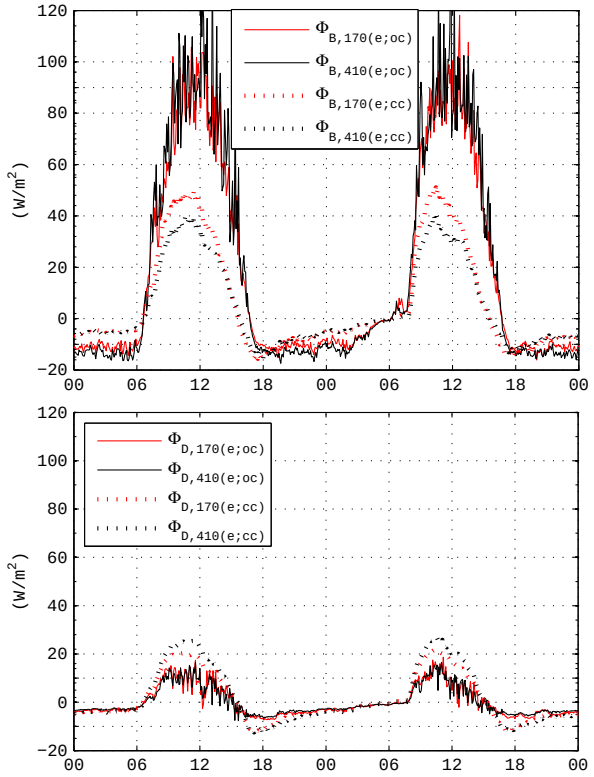

FIGURE *12: Heat flux measured in layers B and D for naturally ventilated and non-ventilated cavities(incoming fluxes are positive)*

the cavity.

Referring to FIGURES 14 the balance pressure around the loop reads :

$$\Delta P_{eb-e} + \Delta P_{e-s} + \Delta P_{s-eh} + \Delta P_{eh-eb} = 0 \qquad (1)$$

Equation (2) can also be write as the balance of pressure losses occurring at inlet ,outlet cavity and along the channel with driving buoyancy and wind effect.

$$\Delta P_b + \Delta P_w = \Delta P_{friction} + \Delta P_{singular} \qquad (2)$$

With,

$$\Delta P_b = gL\sin(\alpha)\rho_M\beta\left(\overline{T_C^\star} - T_{ext}\right) \qquad (3)$$

$$\Delta P_w = Input \qquad (4)$$

$$\Delta P_{friction} = \frac{1}{2}\lambda\frac{L}{D_H}.\frac{\dot{m}^2}{\rho S_c^2} \qquad (5)$$

According to Reynolds turbulent limit calculated from the Nikradse formula, friction factor are evaluated by the low of Hagen-Poiseille or formulated according to the formulation of Al'tsul.

$$\Delta P_{singular} = \frac{1}{2}\rho_{us}\zeta V_{us}^2 = \frac{1}{2}\zeta\frac{\dot{m}^2}{\rho_{us}S_c^2} \qquad (6)$$

Conservative mass flow rate (7),

$$\dot{m} = V\rho S_c = \dot{m}_i = \dot{m}_o \qquad (7)$$

The outlet temperature is given by

$$T_{C,o} = \left(T_{C,i} - \frac{C_2}{C_1}\right)\exp^{-C_1 L} + \frac{C_2}{C_1} \qquad (8)$$

where,

$$C_1 = \frac{wL(h_{c_B} + h_{c_D})}{|\dot{m}|Cp} \qquad (9)$$

and,

$$C_2 = \frac{w\left(T_B h_{c_B} + T_D h_{c_D}\right)}{|\dot{m}|Cp} \qquad (10)$$

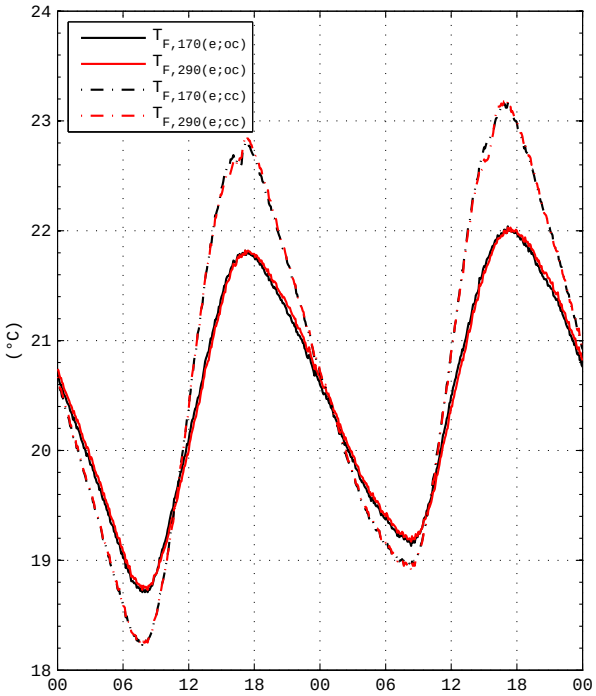

FIGURE *13: Comparison of the surface temperature of the ceiling (upper graph) and air in the room of both cells (lower graph)*

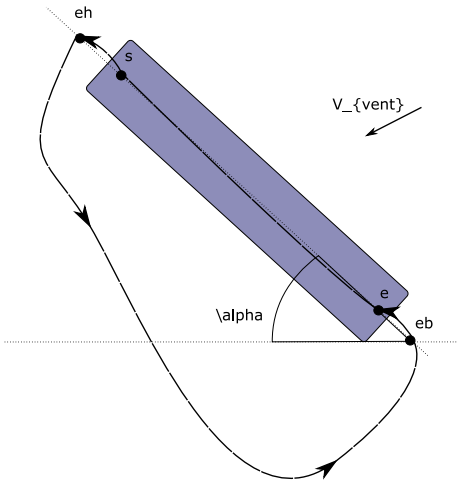

FIGURE *14: Schematic diagram of a cavity*

The average temperature $\overline{T_C^\star}$ is a variable of the model (Eq (3), (13), (14), (15)). [1]

The interior net radiation exchange between both sides of the cavity is given by (11)

$$\phi_{net_{B-D}} = \frac{S_B \sigma_0 ((T_B + 273.15)^4 - (T_D + 273.15)^4)}{\frac{1}{\varepsilon_B} + \frac{1}{\varepsilon_D} - 1} \quad (11)$$

The Nusselt calculation is done through experimental correlation given by (Chami 2009), where Nusselt depend on Prandtl and Rayleigh number. Its field of validity ($30 < \alpha < 45, \quad 0.01 < \frac{B}{L} < 0.03$) is compatible with our application ($\frac{B}{L} = 0.019, \alpha = 30$).

$$Nu_b = 0.796 \left(\frac{b}{L} Ra_b \cos(90 - \alpha) \right)^{0.25} \quad (12)$$

Finally heat balance equation from each sides (13 & 15) and internal air volume (14) are writed

$$\varphi_B = h_{c_B}(T_B - \overline{T_C^*}) + \varphi_{net_{B-D}} \quad (13)$$

$$Lwb\rho C_p d\overline{T_C^*} = h_{c_B} S(T_B - \overline{T_C^*}) - h_{c_D} S(\overline{T_C^*} - T_D) + \dot{m} C_p (T_{C,o} - T_{C,i}) \quad (14)$$

$$\varphi_D = h_{c_D}(\overline{T_C^*} - T_D) + \varphi_{net_{B-D}} \quad (15)$$

NUMERIC & EXPERIMENTAL

Heat transfer in the cavity was numerically evaluated by setting spatial averages of surface temperatures and pressure differences as input of the model. [2]. To make the comparison easier, input solicitations and experimental results were smoothed. Simulations presented in this paper take into account model input parameters uncertitude. We assumed that radiative properties of the downward low emissivity layer could differ from the measured values due to dust deposits. (M.Meury 1960) guide was used to found the more appropriated value for discharge coefficient ζ and friction factor Δ. Several adapted values are listed in TABLE 1. ΔP inaccuracy come from an estimation of the measurement error. We add a common possible offset on both input surfaces temperatures.

We used SimLab (SimLab) and its implemented LHS method (Latin Hypercube Sampling) for generating a [7x100] matrices input parameters. These inputs was then used in SimSPARK model. Mean value from one hundred

1. It is also possible to express the average temperature of the following form : $\overline{T} = \gamma T_{C,o} + (1-\gamma) T_{C,i}$ with $\gamma = 1/(1 \exp^{-\vartheta L}) - 1/(\vartheta L) = (\overline{T_C} - T_{C,i})/(T_{C,o} - T_{C,i})$. The parameter gamma, also called stratification parameter, giving the shape of the temperature distribution along the cavity. A constant value of 0.75 and 0.74 are commonly adopt in work related to solar chimney performance study ((Hirunlabh et al. 1999) and (Ong and Chow 2003)). (Zalewski 1996) compares the average temperature calculation according to the equation (refTfm1) and by taking *gamma* = 0.5 (linear evolution) with experimental data. Conclusion is that weak differences between the two distributions were observed and best fit is obtained considering the linear profile.

2. $T_{B,170(e,oc)}$ and $T_{D,170(e,oc)}$ represented in FIGURES 11 were not used for this surface input average.

simulations and 95 % confident bound for each time step were plotted. The uncertainty range is set voluntary wide. If measured values were inside numerical bounds then this results were used by mean of an optimization technique in order to found the values that best fit the experimental results. If there not, we could assumed that the adopted model was not appropriate or some measurement error occur.

The calculation time step was fixed according to 5-minute averages of experimental data. The calculated heat fluxes (mean and confidante bound) $\{\varphi_{B(n;oc)}, \varphi_{D(n;oc)}\}$ are compared to measurements recorded on both sides at 410 cm from the inlet $\{\varphi_{B,410(e;oc)}, \varphi_{D,410(e;oc)}\}$.

TABLE *1: List of uniform distribution intervals used as input for simulation*

Parameters	Interval
Δ	$[0.15-0.7]mm$
ΔP	$\pm 0.3Pa$
ΔT	$\pm 1°C$
ζ_{in}	$[0.4-0.6]$
ζ_{out}	$[0.7-0.9]$
ε_B	$[0.84-0.93]$
ε_D	$[0.16-0.4]$

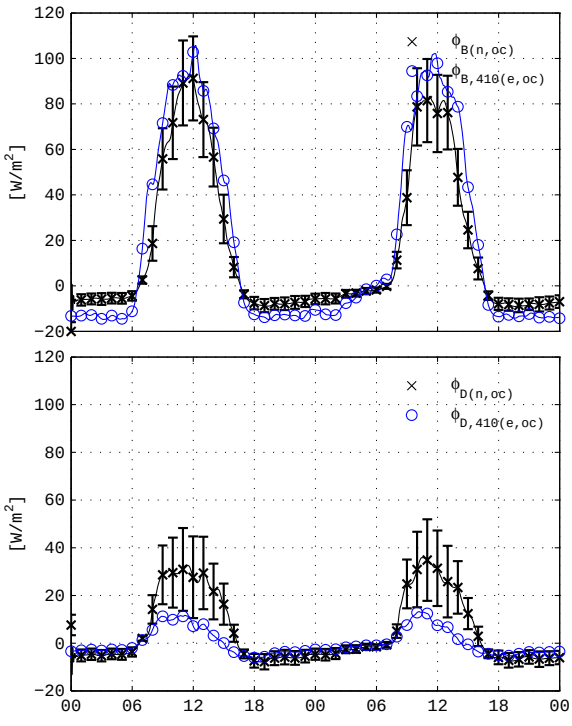

FIGURE *15: Comparison of the computed (black) and measured (blue) heat flux*

As shown in FIGURES 15, the calculated upper flux band includes the experimental results during day time. During night time, model underestimates the heat flux. The bottom graph show the inner flux profile (φ_D). We can observe important differences between experimental results and numerical calculations. Since temperatures and heat fluxes on each side of the cavity were measured, it was possible to calculated net radiation by using Eq.11. Then experimental convective flux for a defined range of emissivity (FIGURES 16) was deduced.

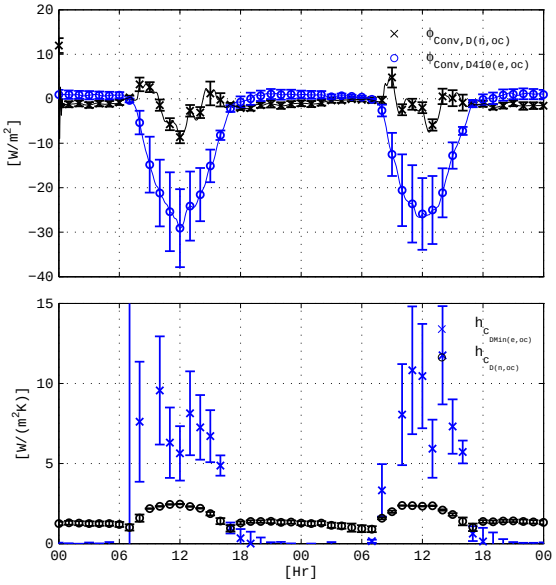

FIGURE *16: Comparison of the inner side convective heat flux and convective transfer coefficient (computed : black, measured : blue).*

Since the numerical and experimental net radiations were calculated with this same assumption it could be assumed that the inner convection is probably the responsible of the differences between calculated and measured inner heat flux. It seems that model underestimated the convective heat transfers. One reasons of such a limited heat transfer could be the calculation method based only on temperature difference between cavity mean air and inner surface temperature ($Nu_b = f(Nu, Gr)$). These differences are measured and could be seen in FIGURES 11.

On the basis of the measured heat flux and in the case of the highest ($\Delta T = T_{C,i(e,oc)} - T_{D,410(e,oc)}$) it was possible to deduced the smallest heat transfer coefficient. The obtained value is higher than calculated one by a factor 3.

Since air circulation is notably governed by wind pressure differences, we are going to study the possibilities of mixed convection coefficient calculation that depend on Reynolds number as well.

CONCLUSION

Heat transfer in timber-frame building envelopes was experimentally assessed under real climatic conditions. A full-scale experimental setup, consisting of two identical rooms, was a roof naturally ventilated interspace coupled with a 90 mm insulated building envelope which could reduce heat-flux transmission by up to fifty percent. As a consequence, the ceiling surface decreases by up to one degree.

A simple mathematical model based on pressure loop analysis was presented ; it was implemented under SimSpark. As well as many others works related to naturally ventilated inter-space, upper and inner side convection transfer coefficients were calculated according to correlation using Grashof and Prandtl number. Considering the inner part of the cavity that has reduced temperature difference with air. Correlation only based on the Grashof number lead to 3 times differences with its deduced value from experimental measure.

Further works are in progress to improve the numerical side to side heat transfer prediction notably by substituting the natural convection coefficient by a mixed one depending on Grashof, Prandtl and Reynolds numbers.

ACKNOWLEDGMENT

This research was possible thanks to the contribution from the French Environment and Energy Management Agency (ADEME) and the Scientific and Technical Center Centre for Building (CSTB). The authors gratefully acknowledge their support on this project and also extend their thanks to as well as François-Dominique Menneteau, Hébert Sallee and Xavier Faure (Faure 2007).

Références

AboulNaga, M. M., and S. N. Abdrabboh. 2000. "Improving night ventilation into low-rise buildings in hot-arid climates exploring a combined wall-roof solar chimney." *Renewable Energy* 19 (1-2) : 47 – 54.

Aboulnaga, Mohsen M. 1998. "A roof solar chimney assisted by cooling cavity for natural ventilation in buildings in hot arid climates : An energy conservation approach in Al-Ain city." *Renewable Energy* 14 (1-4) : 357 – 363. 6th Arab International Solar Energy Conference : Bringing Solar Energy into the Daylight.

Bansal, N.K., Rajesh Mathur, and M.S. Bhandari. 1994. "A study of solar chimney assisted wind tower system for natural ventilation in buildings." *Building and Environment* 29 (4) : 495 – 500.

Brinkworth, B. J., R. H. Marshall, and Z. Ibarahim. 2000. "A validated model of naturally ventilated PV cladding." *Solar Energy* 69 (1) : 67 – 81.

Chami, Nada. 2009. "Évaluation de l'impact des isolants minces réflechissants dans le bâtiment." Ph.D. diss., Université de Cergy Pontoise, Mines ParisTech.

DTU-31.2. 1993. "Construction de maison et bâtiments à ossature en bois." Technical Report NFP21-204-1, AFNOR.

DTU-41.2. 1996. "Revêtements extérieurs en bois." Technical Report NFP65-210-1, AFNOR.

Faure, Xavier. 2007, Novembre. "Optimisation d'enveloppe hybride pour le bâtiment à haute performance énergètique." Ph.D. diss., Universite Joseph Fourrier.

Hirunlabh, J., W. Kongduang, P. Namprakai, and J. Khedari. 1999. "Study of natural ventilation of houses by a metallic solar wall under tropical climate." *Renewable Energy* 18 (1) : 109 – 119.

Hirunlabh, Jongjit, Sopin Wachirapuwadon, Naris Pratinthong, and Joseph Khedari. 2001. "New configurations of a roof solar collector maximizing natural ventilation." *Building and Environment* 36 (3) : 383 – 391.

Khan, Naghman, Yuehong Su, and Saffa B. Riffat. 2008. "A review on wind driven ventilation techniques." *Energy and Buildings* 40 (8) : 1586 – 1604.

Khedari, Joseph, Weerapong Mansirisub, Sompong Chaima, Naris Pratinthong, and Jongjit Hirunlabh. 2000. "Field measurements of performance of roof solar collector." *Energy and Buildings* 31 (3) : 171 – 178.

Lawrence-Berkeley-National-Laboratory, and Ayres-Sowell-Associates. 2003. *SPARK 2.0 reference manual*.

MartIHerrero, J., and M.R. HerasCelemin. 2007. "Dynamic physical model for a solar chimney." *Solar Energy* 81 (5) : 614 – 622.

Miranville, Frédéric. 2002, décembre. "Contribution á l'étude des parois complexes en physique du bâtiment." Ph.D. diss., Université de la Réunion.

M.Meury. 1960. "I.E IDEL'CIK, Memento des pertes de charge." traduction francaise.

Ong, K. S., and C. C. Chow. 2003. "Performance of a solar chimney." *Solar Energy* 74 (1) : 1 – 17.

Sakonidou, E.P., T.D. Karapantsios, A.I. Balouktsis, and D. Chassapis. 2008. "Modeling of the optimum tilt of a solar chimney for maximum air flow." *Solar Energy* 82 (1) : 80 – 94.

SimLab. *SimLab site : http ://simlab.jrc.ec.europa.eu/*.

Zalewski, Laurent. 1996. "Études thermiques expérimentale et simulation numérique d'un mur solaire composite, optimisation des performances énergétiques." Ph.D. diss., Université d'Artois.

NOMENCLATURE

w	width of air channel $[= 0.55m]$
L	length of air channel $[m]$
b	inter - plate spacing $[m]$
S_c	cavity cross-section area $[m^2]$
S	plates area $[= Lwm^2]$
ΔP_b	driving pressure due to buoyancy $[Pa]$
ΔP_w	driving pressure due to the wind effect $[Pa]$
$\Delta P_{friction}$	pressure drop due to friction $[Pa]$
$\Delta P_{singular}$	pressure drop due to singular loss $[Pa]$
$\overline{T_C}$	mean temperature of air channel $[^\circ C]$
$\overline{T_C^*}$	independant mean air temperature of air channel $[^\circ C]$
$\dot{m}$	massique flow rate $[kgs^{-1}]$
h_{c_B}	convective heat transfert coefficient between cover and air layer $[Wm^{-2}K^{-1}]$
h_{c_D}	convective heat transfert coefficient between wall and air layer $[Wm^{-2}K^{-1}]$
V_w	wind speed $[ms^{-1}]$
g	gravitational constant $[= 9.81ms^{-}2]$

Subscripts

us	upstream values evaluation
i	inlet
o	outlet
ext	external
w	wind
b	buoyancy
B, C, D, F	layers denomination
$50, ect...$	distance from the entry
e	experimental
n	numerical
cc	Closed Cavity
oc	Opened Cavity

Greeksymbols

β	coefficient of expansion of air $[K^{-1}]$
α	cavity slope angle $[= 30^\circ]$
σ	Stefan-Boltzmann constant $[= 5.67 \times 10^{-8} Wm^{-2}K^{-4})]$
ε_B	surface emissivity $[= 0.9]$
ε_D	surface emissivity $[= 0.15]$
ρ	density of air $[kgm^{-3}]$
ϕ	heat flux $[W]$
φ	heat flux per unit surface $[Wm^{-2}]$

Dimensionless terms

Pr	Prandtl Number $[Cp\mu/\lambda]$
Re	Reynolds Number $[D_h V/\nu]$
Nu	Nusselts Number $[h_l D_c/\lambda]$
Ra	Rayleight number $[GrPr]$
Gr	Grashof number $[g\beta\Delta T D^3/v^2]$

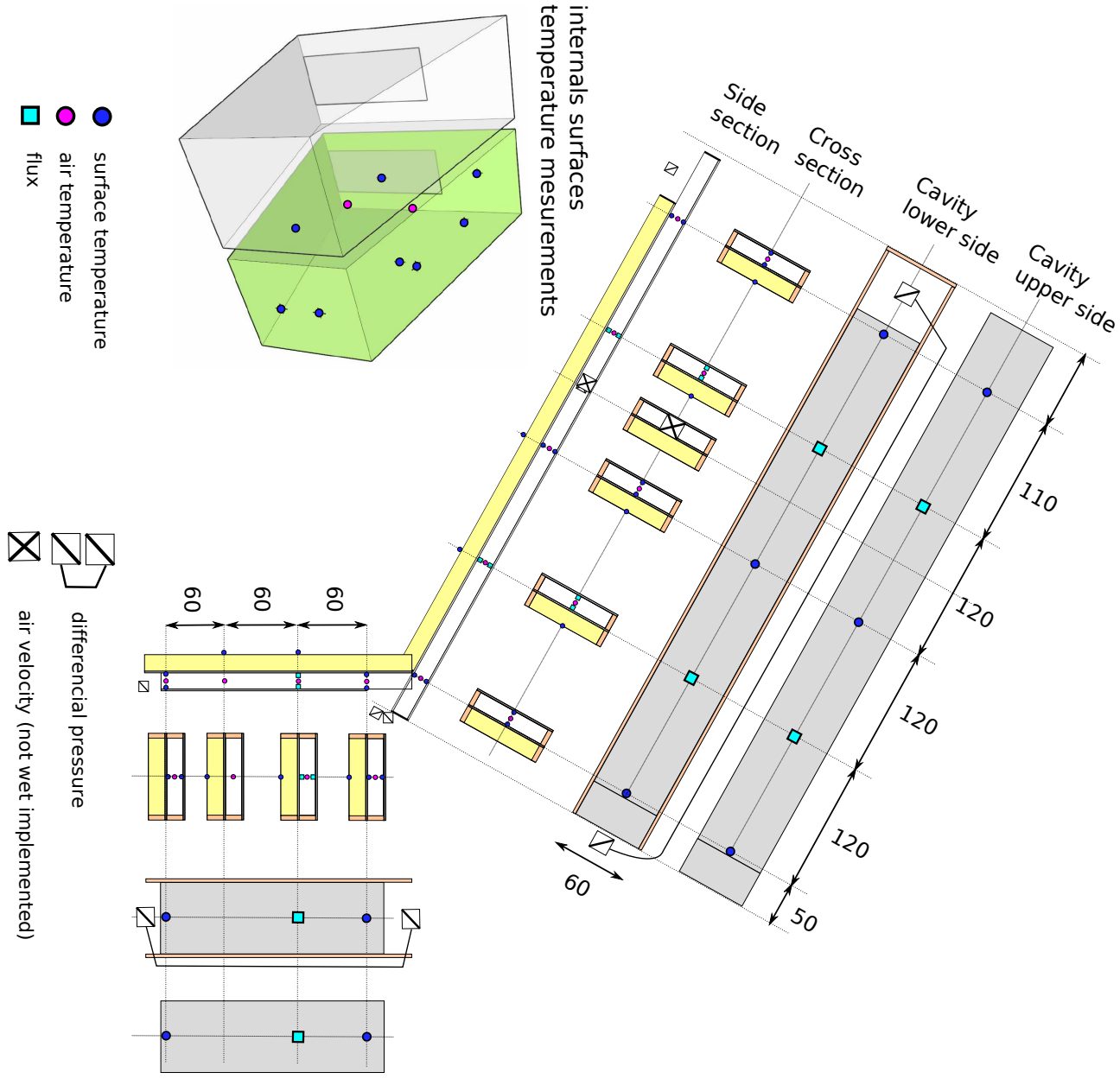

FIGURE *17: ANNEXE : Positions of the measurements in the test cell*